Acta Crystallographica Section A
Foundations of Crystallography
ISSN 0108-7673

Received 30 April 2004
Accepted 13 October 2004

Molecular dynamics investigations of modulated phases in organic materials

Yuansheng Pan* and Gervais Chapuis

Ecole Polytechnique Fédérale de Lausanne Laboratoire de Cristallographie, BSP, 1015 Lausanne, EPFL, Switzerland. Correspondence e-mail: yuansheng.pan@epfl.ch

In order to apply the molecular dynamics (MD) method to simulate modulated phases in organic materials, a compensating external pressure tensor is proposed to compensate for the deficiencies of the force field applied in the simulation. MD can well reproduce modulated phases that have been measured by diffraction. Mechanisms of incommensurate modulation are revealed from the simulations. Details of the structures relating to the origins and mechanisms giving rise to the formation of modulated phases are presented.

1. Introduction

Since its introduction in the 1950s (Alder & Wainwright, 1957) and 1960s (Gibson *et al.*, 1960; Rahman, 1964), molecular dynamics (MD) has become not only a powerful method to understand and interpret experimental results of solids, liquids and gases at the microscopic level, but also for exploring regions that are not experimentally accessible or too costly to perform (Berendsen, 1986; Allen & Tildesley, 1987; Hoover, 1991; Rapaport, 1995). With the development of modern high-performance computers (HPC), this method has been extensively used in the past few decades in physics, chemistry and biology (Ciccotti & Hoover, 1986; Catlow *et al.*, 1990; Allen & Tildesley, 1993; Karplus & McCammon, 2002; Banci, 2003).

The principle of MD simulation is to calculate the forces acting on the atoms in a molecular or other system and analyze their motion. If all details on the motion of the individual atoms in the system are known, it is possible to deduce the bulk properties of the material. These properties include, among others, the structure (*e.g.* crystal structure, predicted X-ray and neutron diffraction patterns), thermodynamics (*e.g.* energy, temperature, pressure) and transport properties (*e.g.* thermal conductivity, viscosity, diffusion). In addition, molecular dynamics can be used to investigate the detailed atomistic mechanisms underlying these properties and compare them with experiment or theory. It is a valuable bridge between experiment and theory.

Incommensurate modulated structures belong to the class of aperiodic crystals (de Wolff, 1974, 1977; Janner & Janssen, 1977; Janssen & Janner, 1987). These materials are characterized by a well defined long-range order but lack three-dimensional periodicity. Their diffraction patterns contain sharp peaks that cannot be indexed with three integers. It is however possible to increase the number of integers in order to completely index a diffraction pattern given a suitable choice of basis vectors (de Wolff, 1974). Their crystal structures cannot be described on the basis of a unit cell and lattice periodicity. Instead, a superspace description of the structure must be used to analyze incommensurately modulated structures (Janner & Janssen, 1977, 1979, 1980; Janssen & Janner, 1987). The origin of incommensuration in crystals has been studied in the past using various theoretical models (Elliott, 1961; Selke & Fisher, 1979; Janssen & Tjon, 1982; Janssen & Janner, 1987; Pimenta & Licinio, 1994; Luk'yanchuk *et al.*, 1994; Neubert *et al.*, 1998).

The technique of molecular dynamics simulation has been used to simulate incommensurate crystals. Parlinski & Chapuis have simulated simple models of incommensurate structures and their transitions between commensurate or incommensurate phases (Parlinski & Chapuis, 1993, 1994). Their model consisted of a very large three-dimensional array of a single point atom placed on a hexagonal lattice. Each atom could only move along the direction parallel to the hexagonal axis. Starting from a potential with harmonic and anharmonic terms, many examples of transition types observed experimentally could be simulated. The principal merits of these studies were that the precise nucleation processes involved in the transition mechanisms could be identified. The influence of temperature or pressure on the phase-transition mechanisms could also be studied which allowed the establishment of complete phase diagrams.

2. MD method and potentials

2.1. MD method

Molecular dynamics (MD) is a simulation technique, which gives the time evolution of a set of interacting atoms by integrating their equations of motion. Newton's equations of motion provide the basis for molecular dynamics. Each atom i in a molecular system is subject to Newton's law:

$$\mathbf{F}_i = m_i \partial^2 \mathbf{r}_i / \partial t^2.$$

Here m_i is the atom mass, $\mathbf{F}_i$ is the acting force from other atoms and $\mathbf{r}_i$ is the position of atom i at time t. The time evolution of the atom positions and velocities can be deter-

mined from this equation provided that initial values are given.

In the absence of external fields, the force $\mathbf{F}_i$ can be assumed to be derivable from a potential of interaction $E(\mathbf{r}_1,\mathbf{r}_2,\ldots,\mathbf{r}_n)$ for each degree of freedom. The force will then be

$$\mathbf{F}_i = -\partial\frac{\partial E(\mathbf{r}_1,\mathbf{r}_2,\ldots,\mathbf{r}_n)}{\partial \mathbf{r}_i}.$$

The equations of motion can be solved analytically only in a few simple cases. When the system involves a large number of complex variables, a computer has to be employed to solve these equations numerically. The molecular dynamics method solves Newton's equations of motion for atoms by taking a small time step and using approximate numerical methods to predict the new atom positions and velocities at the end of the step.

The most popular integration algorithm used in molecular dynamics is the Verlet algorithm, which possesses many advantages. Among others, we can mention accuracy, stability, simplicity, speed and economy (Verlet, 1967, 1968). The Verlet leapfrog algorithm (Feynman *et al.*, 1963) is a widely used version that needs to store only one set of positions and one set of velocities for the atoms. The coding is also simpler to implement.

$$\begin{aligned}\mathbf{V}_{n+1/2} &= \mathbf{V}_{n-1/2} + (\mathbf{f}_n/m)\Delta t + \mathrm{O}(\Delta t^3)\\ \mathbf{r}_{n+1} &= \mathbf{r}_n + \mathbf{V}_{n+1/2}\Delta t + \mathrm{O}(\Delta t^4)\\ \mathbf{V}_n &= \tfrac{1}{2}[\mathbf{V}_{n+1/2} + \mathbf{V}_{n-1/2}] + \mathrm{O}(\Delta t^2)\end{aligned}.$$

Here, $\mathbf{V}_n$ and $\mathbf{f}_n$ are the velocity and the force acting on an atom at time step n. The upper limit of the time step used to solve the equation of motion is determined by the highest frequency motions such as the stretching motions of C—H, O—H and N—H bonds in the system. In our simulations, the time step is set to about 1 fs.

2.2. Potentials (force field) and parameters

The forces in the equation of motion are calculated from potentials (or force fields). The commonly used force fields for describing molecules include a combination of internal coordinates and terms (bond distances, bond angles, torsions *etc.*) to describe the bonding part of the potential energy, and non-bonding terms to describe the van der Waals and electrostatic interactions between atoms (MSI, 1998). The goal of a force field is to describe entire classes of molecules with reasonable accuracy. From the empirical data based on a small set of molecules, it is extended to a larger set of related molecules and structures.

The potential energy of an organic system can be expressed as a sum of valence and non-bonding interactions.

$$E_{\mathrm{total}} = E_{\mathrm{valence}} + E_{\mathrm{nonbond}}.$$

The energy of valence interactions includes bond stretching, valence-angle bending, dihedral-angle torsion and out-of-plane interactions.

$$E_{\mathrm{valence}} = E_{\mathrm{bond}} + E_{\mathrm{angle}} + E_{\mathrm{torsion}} + E_{\mathrm{oop}}.$$

With the bond-stretching energy, atom pairs forming a chemical bond can be kept apart at a fixed distance by a rigid constraint

$$|\mathbf{r}_{ij}|^2 - \mathbf{b}_0^2 = 0$$

or, alternatively, quite close to it by a harmonic spring potential

$$E_{\mathrm{bond}}(|\mathbf{r}_{ij}|) = \tfrac{1}{2}k_b(|\mathbf{r}_{ij} - \mathbf{b}_0|)^2.$$

The bond angles are maintained close to their equilibrium values. The angle bending potential has the following expression:

$$E_{\mathrm{angle}}(\theta) = \tfrac{1}{2}k_\theta(\cos\theta - \cos\theta_0)^2.$$

The bond angle is defined by the positions of three contiguous atoms, *i.e.* $\{i, j, k\}$ with i bonded to j and j bonded to k ($i \neq k$),

$$\cos\theta = (\mathbf{r}_{ij}\cdot\mathbf{r}_{kj})(|\mathbf{r}_{ij}||\mathbf{r}_{kj}|).$$

Similarly, given four contiguous atoms in a molecule, torsion potentials are used to represent restricted rotation around the dihedral angles:

$$E_{\mathrm{torsion}}(\tau) = \sum_{m=0}^{6} C_m\cos^m\tau,$$

where

$$\cos\tau = -\frac{(\mathbf{r}_{ij}\times\mathbf{r}_{jk})\cdot(\mathbf{r}_{jk}\times\mathbf{r}_{kl})}{|\mathbf{r}_{ij}\times\mathbf{r}_{jk}||\mathbf{r}_{jk}\times\mathbf{r}_{kl}|}.$$

The motion of central trivalent atoms in planar groups is restricted using an out-of-plane potential of the form

$$E_{\mathrm{oop}}(s) = \tfrac{1}{2}k_{\mathrm{oop}}s^2$$

with

$$s = \mathbf{r}_{ji}\frac{(\mathbf{r}_{jk}\times\mathbf{r}_{jl})}{|\mathbf{r}_{jk}\times\mathbf{r}_{jl}|}.$$

The energy of interactions between non-bonded atoms accounts for van der Waals and electrostatic energies.

$$E_{\mathrm{nonbond}} = E_{\mathrm{vdW}} + E_{\mathrm{Coulomb}}.$$

In our MD simulations, the van der Waals energy is the Lennard-Jones (LJ) 9-6 potential

$$E_{\mathrm{LJ}}(|\mathbf{r}_{ij}|) = A_{ij}|\mathbf{r}_{ij}|^{-9} - B_{ij}|\mathbf{r}_{ij}|^{-6}$$

and the Coulombic potential satisfies the following expression:

$$E_{\mathrm{Coulomb}}(|\mathbf{r}_{ij}|) = q_iq_j/(4\pi\varepsilon_0|\mathbf{r}_{ij}|).$$

The three dimensions (3D) parallel MD program *ddgmq* (Brown *et al.*, 1997) which was principally designed for the simulation of dense materials is used in our simulations, with periodic boundary conditions. This code is particularly adapted for parallel HPC. The shape and size of the primary MD box is defined by a 3×3 matrix $\mathbf{H}$ made up from the three basis (column) vectors $\{\mathbf{a}, \mathbf{b}, \mathbf{c}\}$ which allows for non-orthogonal cells. All the high-frequency modes associated with H atoms in CH_3 and CH_2 groups can be removed using special constraints (Hammonds & Ryckaert, 1991).

After testing several force fields, parameters of the consistent force field (CFF) (Maple *et al.*, 1994; Hwang *et al.*, 1994) were taken for all our MD simulations. In CFF, a large number of force-field parameters are accurately determined by fitting the energy expression to quantum observables (based on quantum-mechanics calculations and molecular simulations). Non-bonded parameters are calculated by fitting to experimental crystal lattice constants and sublimation energies (Hagler *et al.*, 1979*a*,*b*). The applied parameters are especially adapted for acetals, acids, alcohols, alkanes, alkenes, amides, amines, aromatics, ethers and esters (Maple *et al.*, 1994; Hwang *et al.*, 1994). This force field has been used to successfully predict lattice parameters, r.m.s. atomic coordinates and sublimation energies for crystals.

The partial charges assigned automatically by the selected force field (CFF) are identical for the same type of atom independent of their neighbouring atoms. This is not sufficient for our simulation. In order to improve these parameters, we used the charge equilibration approach implemented in the *Cerius2* package (Rappé & Goddard, 1991; *Cerius2*, 1997), which gives more appropriate values for the molecular geometry and the atomic electronegativities. This approach allows the charges to respond to changes in the environment. The resulting values are in good agreement with the experimental dipole moments and with the result from the electrostatic potentials of accurate *ab initio* calculations (Rappé & Goddard, 1991).

Using as initial model the structure refined from diffraction data and random velocities assigned for the temperature, the MD system can be simulated either at constant-volume constant-temperature (NVT) conditions (Berendsen *et al.*, 1984) or alternatively a required pressure tensor can be applied to give NPT dynamics (Brown & Clarke, 1991). In this case, differences between the internally measured pressure tensor and the externally required pressure tensor may lead to changes in both the box size and shape.

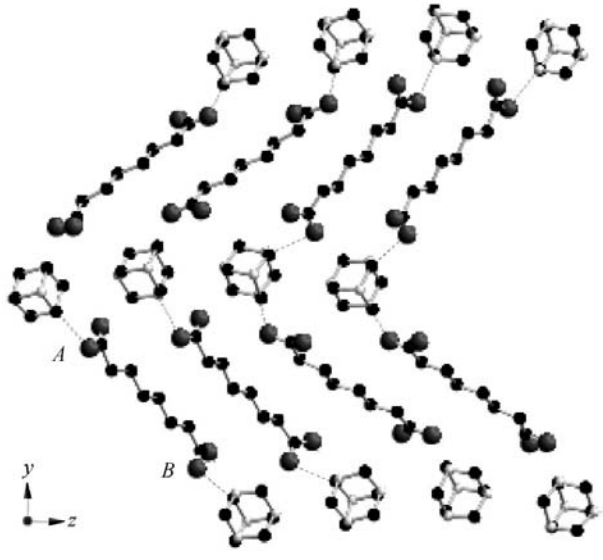

Figure 1
Commensurate crystal structure approximation of hexamethylenetetramine suberate.

After the MD system reaches the required state, many physical properties that usually are a function of the atom coordinates and velocities can be obtained from the simulation results. In particular, quantities such as temperature, energies, density, pressure, mean square displacement, pair distribution function and diffraction patterns can be derived. The simulation result also provides structural details for the specific state.

3. Challenge from diffraction results

Nowadays, the accuracy of diffraction measurements can reach 0.01 Å for lattice constants. Usually, the lattice constants change about ~1% with a temperature change of hundreds of kelvin. Most phase transitions of organic crystals occur within 10 K. If MD simulation is adopted to reproduce these phase transitions, the accuracy of the simulation should be sufficiently high to distinguish these phases.

However, owing to the application of generic potentials (or force field), the accuracy of MD simulation is usually worse than 5% for lattice parameters (Pan *et al.*, 2002). It is thus almost impossible to reproduce the experimental structure with the same accuracy. The same problem also exists for reproducing phase transitions in crystals that have been determined experimentally.

In order to solve this problem, the first step is to reproduce the same structure as measured experimentally. An external pressure tensor field is introduced to compensate for the deficiencies of the selected force field (Pan *et al.*, 2003). This guarantees that MD simulation can well reproduce the experimental measurements. This can be justified with the following argument. The equation of state of an N-atom system can be represented by a virial expression (Haile, 1992):

$$\mathbf{P}V = \sum_{i=1}^{N} m_i \dot{\mathbf{r}}_i \dot{\mathbf{r}}_i + \sum_{v}^{\text{all force on } i} \mathbf{r}_i^{(v)} \mathbf{f}_i^{(v)}.$$

With bonding and non-bonding interactions used in potentials, the pressure tensor can be represented as (see Brown & Neyertz, 1995)

$$\mathbf{P} = \left\{ \frac{1}{V} \sum_{i=1}^{N} m_i \dot{\mathbf{r}}_i \dot{\mathbf{r}}_i \right\} + \mathbf{P}_{\text{bond}} + \mathbf{P}_{\text{nonbond}}.$$

If in this equation the assigned pressure is the normal pressure, the volume of the system does not usually agree with the experimental results. A compensating external pressure tensor is therefore needed to correct the deficiencies in the applied force field in order to reproduce the experimental lattice parameters in the fixed-temperature MD simulation (Pan *et al.*, 2003). With the compensating external pressure tensor applied, the volume can be written as follows.

$$V \equiv V_{\text{exp}} = \frac{\sum_{i=1}^{N} m_i \dot{\mathbf{r}}_i \dot{\mathbf{r}}_i}{\mathbf{P} + \mathbf{P}_{\text{compen}} - \mathbf{P}_{\text{bond}} - \mathbf{P}_{\text{nonbond}}}$$

The new equation of state becomes

$$\mathbf{P} + \mathbf{P}_{\text{compen}} = \left\{ \frac{1}{V} \sum_{i=1}^{N} m_i \dot{\mathbf{r}}_i \dot{\mathbf{r}}_i \right\} + \mathbf{P}_{\text{bond}} + \mathbf{P}_{\text{nonbond}}.$$

In MD simulations, this compensating pressure tensor can be obtained by running NVT simulations to equilibrium from the refined structure. A NPT simulation is then carried out to adjust the system to the required state by applying the compensating pressure tensor. The MD simulations can thus well reproduce the experimental structures at starting temperatures (Pan *et al.*, 2002, 2003; Pan, Birkedal *et al.*, 2004; Pan, Brown *et al.*, 2004*a*). This gives also the possibility to reproduce the observed phase transition occurring not too far from the starting temperature.

4. MD simulations of the modulated phase in hexamethylenetetramine suberate

The organic compound hexamine suberate is a layer structure with alternating sheets of hexamine and suberic acid linked by hydrogen bonds between N and O atoms (Fig. 1). At room temperature, hexamine suberate is strongly modulated as witnessed by satellite reflections up to sixth order. The incommensurate modulation is very stable between 120 and 300 K (Gaillard *et al.*, 1996, 1998). The incommensurate structure has been refined in superspace. Displacive atomic modulations including up to eight harmonics lead to satisfactory models. The analysis of the refinements indicates that, in a layer, the zigzag planes of the acid chains take essentially two orientations, forming an angle of approximately 60°.

4.1. Simulation

The molecular dynamics method is used to investigate the mechanism of commensurate-to-incommensurate phase transition. The starting model with dimensions 180 × 50 × 180 Å was a commensurate approximation of the experimental structure determined at 295 K. The simulation was first carried out under NVT conditions keeping the experimental shape and size of the model. The simulation was performed to reach equilibrium at that temperature and a compensating pressure tensor was then obtained as given in Table 1. At the same temperature, a NPT (constant pressure tensor) simulation was then performed to equilibrate the system with the compensating pressure tensor. The same pressure tensor was also used when the system was heated to 580 K and cooled down to 15 K.

Table 1
The average compensating pressure tensor components (in 10^5 Pa) obtained at 295 K for the hexamethylenetetramine suberate system.

	X	*Y*	*Z*
X	−2130	0	−1240
Y	0	−1520	0
Z	−1240	0	1340

The simulation provides the lattice constants and angles for the different temperatures. Over the whole temperature range, the lattice constants *a*, *b* and *c* agree well with the experimental observations. The experimental and simulated lattice constants and angles are compared at 295 and 123 K. The close agreement at 295 K is due to the application of the compensating pressure tensor. When the system is cooled to 123 K, the largest error in the lattice constants is 0.64%.

4.2. Phase transitions

Phase transitions are investigated by checking the physical properties of the system at different temperatures. In our case, lattice constants and angles of the simulation, density, mean-square displacements and torsion angle energy for the whole temperature range provides the requested information (Pan *et al.*, 2001, 2002). In the crystalline phase, phase transitions are found at about 290 and 150 K.

In order to identify the crystalline phases, single-crystal X-ray diffraction patterns were simulated using the software *DISCUS* (Proffen & Neder, 1997). The resulting diffraction patterns reveal the commensurate, incommensurately modulated and lock-in phases in temperature ranges above 290, 290–150 and below 150 K, respectively. Fig. 2 illustrates the diffraction patterns at 352, 200 and 141 K representing the three different phases, respectively. In the 200 K diffraction patterns, the satellites along the diagonal direction are not

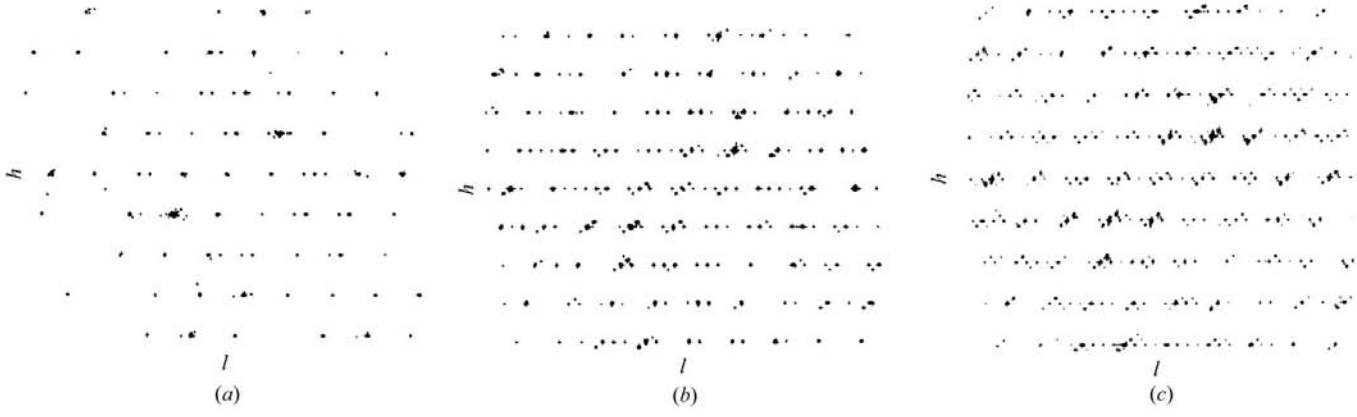

Figure 2
Simulated diffraction patterns at (*a*) 352 K, (*b*) 200 K and (*c*) 141 K.

aligned with the main reflections. This indicates the incommensurate character of the structure.

4.3. Mechanism of incommensurate modulation

In the commensurate phase that is stable between 290 and 410 K, the simulated X-ray diffraction pattern exhibits three satellites between the main reflections along $\mathbf{c}^*$. A very clear long-range ordering (l.r.o.) with a fourfold pattern exists in both HMT and suberic acid layers. The hydrogen bonds between terminal H atoms of suberic acid and N atoms of HMT appear in three consecutive rows; they are absent in the fourth. This absence of hydrogen bonds is the origin of the periodicity of the phase. The displacement of the HMT layers is also modulated with the same periodicity. This l.r.o. is illustrated in Fig. 3(*a*) for the *XY* plane and 3(*b*) for a layer of C-atom chains in the suberic acid structure.

At temperatures below 290 K, new satellites appear in the simulated diffraction pattern. In this temperature range, a new periodicity with $N \simeq 8$ molecules can be clearly observed in both the suberic acid and HMT layers as presented in Figs. 4(*a*) and 4(*b*) at 141 K. In addition, the periodicity obtained in the commensurate phase still exists in the system. Fig. 4(*a*) clearly shows the new periodicity in the orientation of individual C-atom chains of suberic acid and modulated displacement of the HMT layer. Fig. 4(*b*) illustrates the new periodicity in the suberic acid layers. The simulation result shows that the origin of the commensurate–incommensurate phase transition is related to the orientation of the individual C-atom chains of suberic acid. Fig. 5 shows the distribution of the orientations of C-atom chains at 295 and 141 K. From 295 to 141 K, a splitting of each single peak is observed in the orientations of the C-atom chains. This splitting is linked to the new periodicity which is presented in Fig. 4.

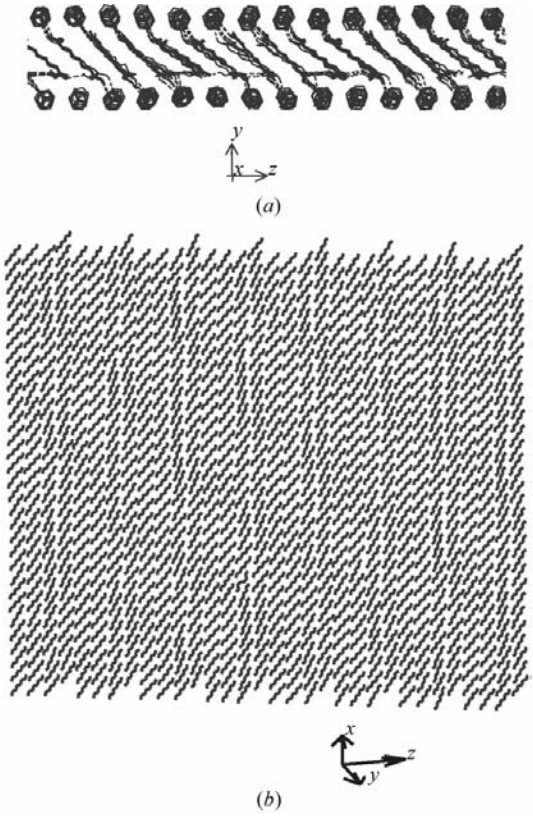

Figure 3
Long-range ordering in the commensurate phase at 352 K.

5. MD simulation of bis(4-chlorophenyl) sulfone (BCPS)

The crystal structure of bis(4-chlorophenyl) sulfone (BCPS) (see Fig. 6) exhibits a continuous structural phase transition from a normal phase to an incommensurately modulated phase (IC) occurring at 150 K (Pusiol *et al.*, 1989). The IC phase is stable from 150 K down to a very low temperature (4.5 K). It has been extensively studied by different experimental techniques, including X-ray diffraction (Kasano *et al.*, 1990; Zúñiga *et al.*, 1993), neutron scattering (Ollivier *et al.*, 1998), NMR (Taye *et al.*, 2002), NQR and Raman spectroscopy (Schneider *et al.*, 2001; Blinc *et al.*, 2002). From elastic neutron measurements, high-order satellite reflections could be measured. An increase of their intensities was also observed on cooling (Etrillard, Even *et al.*, 1993; Etrillard, Toudic *et al.*, 1993). The microscopic mechanism for the

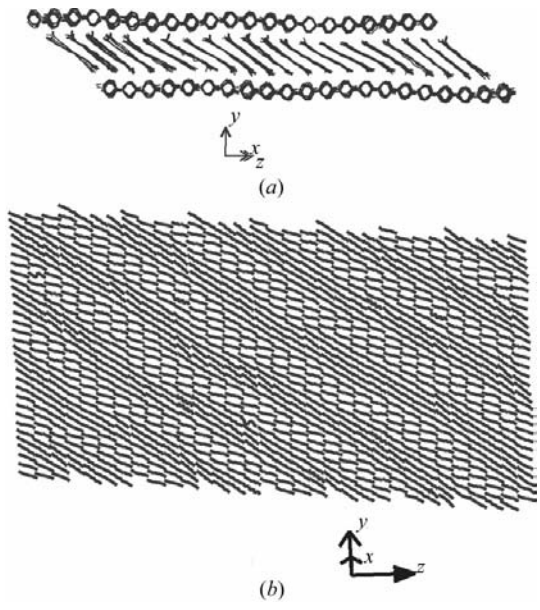

Figure 4
Long-range ordering only found in the incommensurate phase at 141 K.

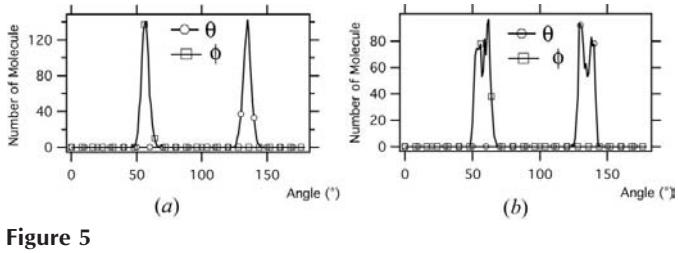

Figure 5
The distribution of the orientations of C-atom chains at (*a*) 295 K and (*b*) 141 K.

incommensurate character of the IC phase was extensively studied. Pusiol *et al.* (1989) proposed that the IC phase was related to the dihedral angle between the two benzene ring planes. Ishit *et al.* (1992) suggested that the incommensurate modulation is linked to the soft mode which shows a significant intramolecular twisting of the phenyl rings in the molecule. X-ray and neutron diffraction have shown that the wavevector of the incommensurate modulation, $\mathbf{q} = -0.78\mathbf{b}^*$, varies smoothly with temperature in the whole IC phase (Kasano *et al.*, 1990; Zúñiga *et al.*, 1993). The IC modulated waves were measured and were related to both atomic displacements and the dihedral and bending angles of the molecule (Zúñiga *et al.*, 1993). Blinc *et al.* (2002) used NQR spin-lattice relaxation to show large-scale fluctuations of the pinned modulation wave instead of small-scale fluctuations (phasons and amplitudons) as the origin of the incommensuration modulation.

5.1. Simulation and results

Molecular dynamics simulation of bis(4-chlorophenyl) sulfone was carried out in order to study the phase transition and mechanism of an IC modulated structure (Pan, Brown *et al.*, 2004*a*,*b*). The starting model of the simulation was taken from the experimentally refined structure at 90 K (Zúñiga *et al.*, 1993), with monoclinic symmetry $I2/a$, $a = 20.20$, $b = 4.910$, $c = 12.054$ Å and $\beta = 90.02^\circ$. The size of the simulated system was $80 \times 160 \times 100$ Å with 102 400 atoms. The system was first run to equilibrium under NVT conditions without changing the lattice parameters. A compensating pressure tensor field was obtained as shown in Table 2. In a second step, constant pressure simulations (NPT) were performed in order to vary the temperature of the system while applying the compensating pressure tensor. The system was heated to 460 K and then cooled to 17 K.

Table 2
The average compensating pressure tensor components (in 10^5 Pa) obtained at 90 K for the bis(4-chlorophenyl) sulfone system.

	X	*Y*	*Z*
X	−1170	20	452
Y	20	−861	−13
Z	452	−13	601

The temperature behaviour of the *a* and *b* lattice constants are plotted in Fig. 7. The simulated lattice parameters agree well with the experiment at 90 K and deviate less than 0.5% at room temperature. The changes in the lattice constants show roughly the same features as in the experiments (Etrillard, Even *et al.*, 1993). However, the simulated phase-transition temperature of 260 K differs from the observed value of 150 K (Etrillard, Even *et al.*, 1993). This temperature shift is due to the characteristics of a generic force field.

The structure above 260 K is the normal commensurate phase. The diffraction pattern of the *hk*0 plane at 300 K is represented in Fig. 8. The diffraction patterns show that the incommensurate phase exists at all temperatures below 260 K. Fig. 9 illustrates the diffraction pattern at 17 K. In the simu-

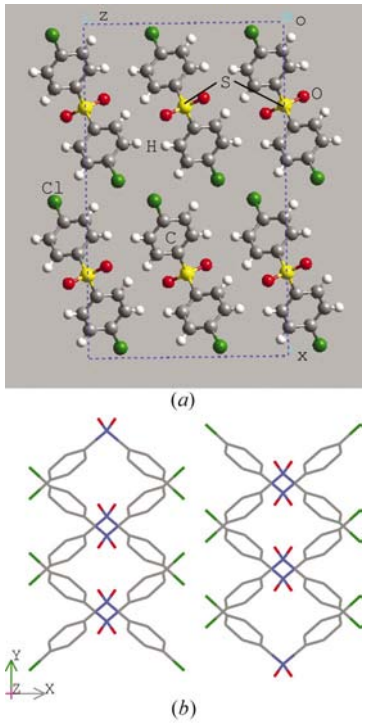

Figure 6
Structure of bis(4-chlorophenyl) sulfone in *XZ* and *XY* planes.

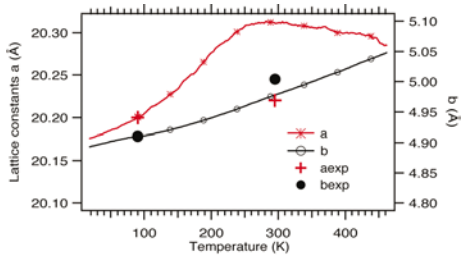

Figure 7
Simulated temperature evolution of lattice constants *a* and *b*.

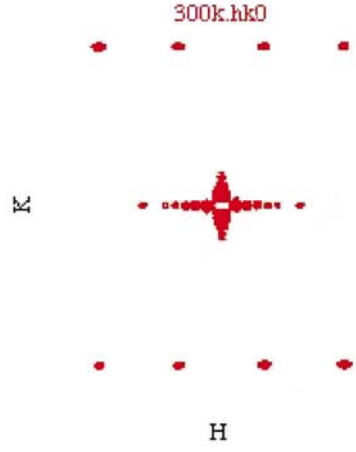

Figure 8
Simulated diffraction pattern *hk*0 at 300 K

lations, the positions of the main reflections and all satellites are in good agreement with the experimental result at 13 K (Kasano *et al.*, 1990; Etrillard, Even *et al.*, 1993). A more detailed comparison of the shape and orientation of the main and first- order satellite reflections also shows good agreement between simulation and experimental data (Zúñiga, 1993). As in previous refinements of the atomic modulation, one modulation vector is supposed to characterize all satellites. The modulation wavevector could be roughly identified as $\mathbf{a}^* + 0.22\mathbf{b}^*$ or $-0.78\mathbf{b}^*$, which are the same as the experimentally measured ones (Kasano *et al.*, 1990; Zúñiga *et al.*, 1993).

5.2. Mechanism of incommensurate modulations

The incommensurate modulation can be identified as displacive and can be represented with only the centre S atom instead of the whole molecule. Two components of the modulated waves are found along **b** in the IC phase. One is a z displacement of S atoms along **y**, as illustrated in Fig. 10(*a*). The wavelength of this modulation is about 5.3 molecules. The phase of this modulation agrees with that of the bending angle from experiment (Zúñiga *et al.*, 1993). Another modulation wave, shown in Fig. 10(*b*), is an x displacement of S along **y**. Its wavelength is about 10.6 molecules. The phase of this modulation agrees with that of the dihedral angle from experiment (Zúñiga *et al.*, 1993). The phases of the two modulated waves are different.

The detailed analysis of the simulated crystalline structure allows one to find the origin of the modulation waves. Intermolecular interactions are found in the formation of O···H bonds along **z** and Cl···H and Cl···Cl bonds along **x** (see Fig. 6). As a consequence of the O···H interactions, we observe a modulation of the intermolecular distance along **y**. This modulation wave result induces a displacement of the molecule along **z** by adapting the bending angle between the two C-atom rings in the same molecule. The x displacement of the S-atom centre is determined by the distances Cl···H, H···Cl and Cl···Cl between the ends of neighbouring molecules. In the IC phase, these distances are modulated along **y**. The result of this modulation wave is to vary the displacement of the molecule along **x** by rotating the phenyl rings. The wavelength of this modulation wave component is the same as that of the x displacement measured at the centre S atoms. This wavelength is twice that of the modulation wave with displacement along **z**. Unfortunately, the refinement of the structure (Zúñiga *et al.*, 1993) does not indicate the relation between the two modulation components owing to the constraints assigned to the second-order harmonics. Our simulation result reveals however that the two modulation components are related to the x and z displacements of the molecules. As revealed by the experimental results (Zúñiga *et al.*, 1993), the changes of torsion and bending angles of two C-atom rings are roughly

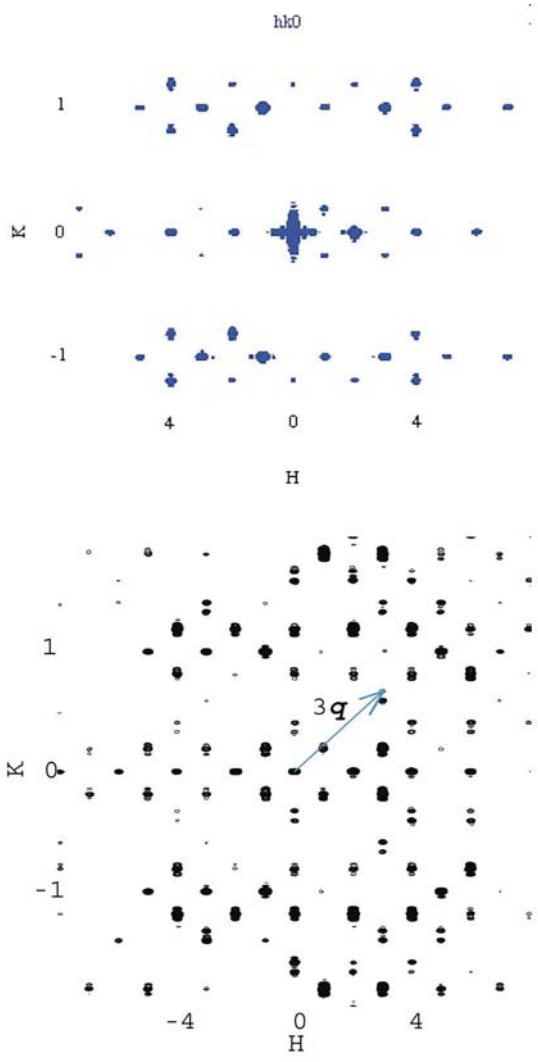

Figure 9
Simulated diffraction pattern at 17 K.

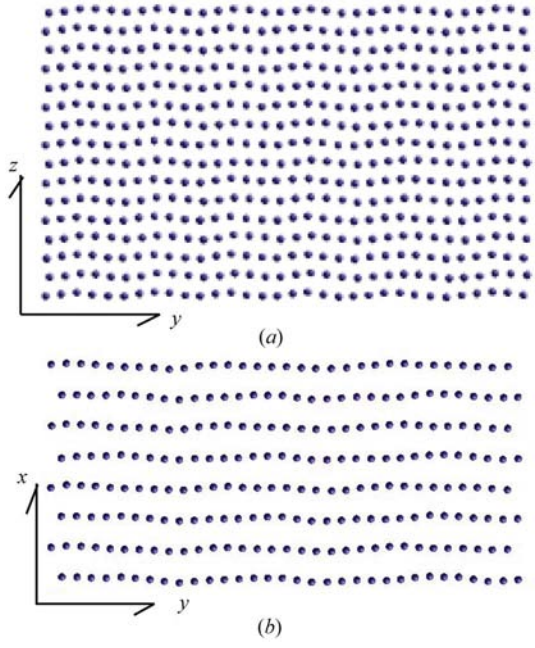

Figure 10
Modulation waves along the b axis: (*a*) in the z displacement; (*b*) in the x displacement.

similar to the z and x displacements, which confirm the two modulation wave components.

6. Conclusions

With the two examples presented above, we have shown that incommensurate structures can be simulated by a molecular dynamics technique with generic force field. In addition, we can also simulate sequences of phase transitions where commensurate and incommensurate phases can occur. We have shown that the pressure tensor can be used to adjust the system in order to reproduce precisely the experimental lattice constants. This tensor remains unchanged over the temperature interval of the simulations. Owing to the aperiodic character of incommensurate structures, the periodic boundary condition obviously has some effect in the simulation of finite objects. If for example the dimension of the system along the modulation wave is smaller than its wavelength, the simulation of course cannot represent the real structure. This effect is accounted for in the design of the simulation box. Several multiples of the modulation wavelength are usually in our simulation system in order to be able to reproduce the behaviour which is observed experimentally.

There are also a certain number of important points to consider in order to reproduce the experimental results. In MD simulations, a physical quantity or structure is determined only after the system reaches equilibrium. A relaxation time is needed for a physical quantity to reach its equilibrium value. If the simulation is initiated from the experimental structure, the relaxation time can vary from the order of tenths to hundreds of ps, depending on the system. In the case of phase transitions, the system starts to be unstable owing to heating or cooling. It then transforms to a new phase, and finally reaches a new equilibrium. In order to reproduce a phase transition in the MD system, a much longer relaxation time is needed for the system to complete all the stages. If the relaxation time is short enough, a well designed simulation is able to reproduce the phase transition. This means the simulation procedure should be treated according to the relaxation time of the studied phenomenon. However, if the relaxation time is much larger than the overall simulation time, the MD technique will certainly fail to reproduce the experimental data characterizing the phase-transition mechanism.

This work was supported by the Swiss National Science Foundation grant No. 20-67698.02. We thank the CSCS in Manno and the IT Domain of the EPFL (Lausanne) for the use of the high-performance computing facilities.

References

Alder, B. J. & Wainwright, T. E. (1957). *J. Chem. Phys.* **27**, 1208.

Allen, M. P. & Tildesley, D. J. (1987). *Computer Simulation of Liquids.* Oxford University Press.

Allen, M. P. & Tildesley, D. J. (1993). *Computer Simulation in Chemical Physics.* Dordrecht: Kluwer Academic Publishers.

Banci, L. (2003). *Curr. Opin. Chem. Biol.* **7**, 143–149.

Berendsen, H. J. C. (1986). *Molecular Dynamics Simulation of Statistical-Mechanical Systems*, edited by G. Ciccotti & W. G. Hoover. Amsterdam: North-Holland.

Berendsen, H. J. C., Postma, J. P. M., van Gunsteren, W. F., DiNola, A. & Haak, J. R. (1984). *J. Chem. Phys.* **81**, 3684–3690.

Blinc, R., Mikac, U., Apih, T., Dolinek, J., Seliger, J., Slak, J., Žumer, S., Guibe, L. & Ailion, D. C. (2002). *Phys. Rev. Lett.* **88**, 015701.

Brown, D. & Clarke, J. H. R. (1991). *Comput. Phys. Commun.* **62**, 360–369.

Brown, D., Minoux, H. & Maigret, B. (1997). *Comput. Phys. Commun.* **103**, 170–186. See also *The gmq User Manual Version 3*, available at http://www.univ-savoie.fr/labos/lmops/fr/index_fr.html.

Brown, D. & Neyertz, S. (1995). *Mol. Phys.* **84**, 577–595.

Catlow, C. R. A., Parker, S. C. & Allen, M. P. (1990). Editors. *Computer Modelling of Fluids, Polymers and Solids.* Dordrecht: Kluwer Academic Publishers.

Cerius2 (1997). Molecular Simulations Inc., San Diego, CA, USA.

Ciccotti, G. & Hoover, W. G. (1986). Editors. *Molecular Dynamics Simulation of Stadistical-Mechanical Systems.* Amsterdam: North-Holland.

Elliott, R. J. (1961). *Phys. Rev.* **124**, 336.

Etrillard, J., Even, J., Sougoti, M., Launois, P., Longeville, S. & Toudic, B. (1993). *Solid State Commun.* **87**, 47.

Etrillard, J., Toudic, B., Bertauld, M., Even, J., Gourdji, M., Péneau, A. & Guibé, L. (1993). *J. Phys. (Paris) I*, **3**, 2437.

Feynman, R. P., Leighton, R. B. & Sands, M. (1963). *The Feynman Lectures on Physics*, Vol. 1. Reading, MA: Addison-Wesley.

Gaillard, V. B., Chapuis, G., Dusek, M. & Petricek, V. (1998). *Acta Cryst.* A**54**, 31–43.

Gaillard, V. B., Paciorek, W., Schenk, K. & Chapuis, G. (1996). *Acta Cryst.* B**52**, 1036–1047.

Gibson, J. B., Goland, A. N., Milgram, M. & Vineyard, G. H. (1960). *Phys. Rev.* **120**, 1229.

Hagler, A., Dauber, T. P. & Lifson, S. (1979*a*). *J. Am. Chem. Soc.* **101**, 5122–5130.

Hagler, A., Dauber, T. P. & Lifson, S. (1979*b*). *J. Am. Chem. Soc.* **101**, 5131–5141.

Haile, J. M., (1992). *Molecular Dynamics Simulation: Elementary Method.* New York: Wiley.

Hammonds, K. D. & Ryckaert, J.-P. (1991). *Comput. Phys. Commun.* **62**, 336–351.

Hoover, W. G. (1991). *Computational Statistical Mechanics.* Amsterdam: Elsevier.

Hwang, M.-J., Stockfisch, T. P. & Hagler, A. T. (1994). *J. Am. Chem. Soc.* **116**, 2515–2525.

Ishit, K., Nakayama, H., Sakato, T. & Kano, H. (1992). *J. Phys. Soc. Jpn*, **61**, 2317–2326.

Janner, A. & Janssen, T. (1977). *Phys. Rev. B*, **15**, 643–658.

Janner, A. & Janssen, T. (1979). *Physica (Utrecht)*, A**99**, 47–76.

Janner, A. & Janssen, T. (1980). *Acta Cryst.* A**36**, 399–408.

Janssen, T. & Janner, A. (1987). *Adv. Phys.* **36**, 519–624.

Janssen, T. & Tjon, J. A. (1982). *Phys. Rev. B*, **25**, 3767–3785.

Karplus, M. & McCammon, J. A. (2002). *Nature Struct. Biol.* **9**, 646–652.

Kasano, H., Koshiba, Kasatani, T. & Terauchi, H. H. (1990). *J. Phys. Soc. Jpn*, **59**, 408.

Luk'yanchuk, I., Jorio, A. & Pimenta, M. A. (1994). *Phys. Rev. B*, **57**, 5086–5092.

Maple, J. R., Hwang, M.-J., Stockfisch, T. P., Dinur, U., Waldman, M., Ewig, C. S. & Hagler, A. T. (1994). *J. Comput. Chem.* **15**, 162–182.

MSI (1998). *Cerius*^{2}. Molecular Simulations Inc., San Diego, CA, USA.

Neubert, B., Pleimling, M. & Siems, R. (1998). *Ferroelectrics*, **208** 141–190.

Ollivier, J., Etrillard, J., Toudic, B., Ecolivet, C., Bourges, P. & Levanyuk, A. P. (1998). *Phys. Rev. Lett.* **81**, 3667.

Pan, Y., Birkedal, H., Pattison, P., Brown, D. & Chapuis, G. (2004). *J. Phys. Chem. B*, **108** 6458–6466.
Pan, Y., Brown, D. & Chapuis, G. (2001). *Ferroeletrics*, **250** 107–110.
Pan, Y., Brown, D. & Chapuis, G. (2002). *Phys. Rev. B*, **65** 184205.
Pan, Y., Brown, D. & Chapuis, G. (2003). *Mol. Simul.* **29**, 509–518.
Pan, Y., Brown, D., Zuniga, F. J. & Chapuis, G. (2004*a*). *Phys. Rev. Lett.* To be published.
Pan, Y., Brown, D., Zuniga, F. J. & Chapuis, G. (2004*b*). *Ferroelectrics*, **305**, 53–56.
Parlinski, K. & Chapuis, G. (1993). *Phys. Rev. B*, **47**, 13983–13991.
Parlinski, K. & Chapuis, G. (1994). *Phys. Rev. B*, **49**, 11643–11651.
Pimenta, M. A. & Licinio, P. (1994). *Phys. Rev. B*, **50**, 722–726.
Proffen, Th. & Neder, R. B. (1997). *J. Appl. Cryst.* **30**, 171–175.
Pusiol, D., Wolfenson, A. E. & Brunetti, A. H. (1989). *Phys. Rev. B*, **40**, 2523.
Rahman, A. (1964). *Phys. Rev.* **136**, A405.
Rapaport, D. C. (1995). *The Art of Molecular Dynamics Simulation.* Cambridge University Press.
Rappé, A. K. & Goddard, W. A. (1991).*J. Phys. Chem.* **95**, 3358.
Schneider, J., Nunes, L. A. & Panepucci, O. H. (2001). *Phys. Rev. B*, **64**, 094103.
Selke, W. & Fisher, M. E. (1979). *Phys. Rev. B*, **20**, 257.
Taye, A., Michel, D. & Petersson, J. (2002). *Phys. Rev. B*, **66**, 174102.
Verlet, L. (1967). *Phys. Rev.* **159**, 98.
Verlet, L. (1968). *Phys. Rev.* **165**, 201.
Wolff, P. M. de (1974). *Acta Cryst.* A**30**, 777–785.
Wolff, P. M. de (1977). *Acta Cryst.* A**33**, 493–497.
Zúñiga, F. J. (1993). Private communication.
Zúñiga, F. J., Pérez-Mato, J. M. & Breczewski, T. (1993). *Acta Cryst.* B**49**, 1060.